Journal of Applied Science and Engineering Methodologies
Volume.2, No.3, (2016): Page.272-277
www.scientistlink.com/jasem

Influence of Lanthanum Doping on the Structural and Optical Properties of Hematite Nanopowders

J. Sharmila Justus[1*], S. Dawn Dharma Roy[2], A. Moses Ezhil Raj[3]

[1]Department of Physics & Research Centre, Women's Christian College, Nagercoil, India.
[2]Department of Physics & Research Centre, Nesamony Memorial Christian College, Marthandam, India.
[3]Department of Physics & Research Centre, Scott Christian College (Autonomous), Nagercoil, India
sharmi.fiziks@gmail.com

Abstract

Rare-earth elements are an attractive class of dopant elements, as they give easily trivalent cations that possibly altering the structure and other properties of the parent nanoparticles and creating multifunctional materials because of their *f*-electronic configurations. Herein, experimental evidence has been given for a better understanding of the factors that dictate the interactions of La doping on the structure and optical properties of iron oxide nanoparticles. For that, lanthanum doped hematite (α-Fe_2O_3) nanoparticles were prepared by a facile solution method using iron (III) chloride ($FeCl_3$) as starting precursor and sodium hydroxide (NaOH) as reducing agent without templates at low temperature. As-prepared powders were subsequently calcined in air for 3 hr at 800 ºC. X-ray diffraction (XRD) technique was used to study the nanocrystal formation of α-Fe_2O_3 and Fourier Transform Raman (FT-Raman) spectral information identified the chemical bond structure of the nanoparticles. Morphology study of the nanoparticles was identified using Scanning Electron Microscope (SEM) and the incorporated La content was recognized from the Energy Dispersive X-ray Spectroscopy (EDS) analysis. The optical absorption spectrum was recorded in the wavelength range of 200-2000 nm and the optical parameters such as absorption coefficient and optical band gap energy of pure and doped Fe_2O_3 nanoparticles were determined. Obtained results are interpreted by considering the impregnation of trivalent La cations that replaced Fe cations of the host structure.

Keywords: *Sol-gel precipitation, nanopowder, XRD, FT-Raman, SEM, Optical*

1. Introduction

Nanosized iron oxides have wide applications in catalysis, magnetic recording, catalysis, field emission devices, spin electronic devices and rechargeable lithium batteries due to its special optical, magnetic and electrical properties [1-6]. Rare earth ions having large magnetic moments and luminescent properties greatly influence the crystal properties [7]. They are used in magnetic resonance imaging (MRI) as contrasting agents [8]. Lanthanum ions are also an interesting candidate possessing unique chemical and physical properties. Mixed oxides having perovskite structure shows interesting properties [9, 10]. Melo et al. have synthesized lanthanum doped Fe_2O_3 pigments from polymeric precursors using Pechini method [11]. Francesca et al. [12] and Gaurav Goyal et al. [13] have studied the modification of magnetic properties of α-Fe_2O_3 on doping Eu and Nd respectively. Here we report a facile solution approach for the synthesis of pure and La doped hematite nanoparticles by simply adjusting the pH of the solution for the first time. The influence of dopant on its structural, surface morphological and optical characterization was systematically presented in this paper.

2. Experimental Procedure

2.1. Synthesis

For the synthesis of pure and lanthanum doped hematite nanoparticles, ferric chloride (AR grade) and ethylene glycol were used as the starting chemicals. Initially, Iron (III) chloride was dissolved in a mixture of deionized water and ethylene glycol at room temperature for a concentration of 0.1M. The obtained solution was reduced using NaOH solution (0.1 M) to get a dark reddish brown clear solution. The pH of this solution was adjusted to be 3 by adding ammonia solution and stirred for 1h at 100ºC and then allowed to precipitate. The obtained precipitates were repeatedly washed with ethanol and distilled water and dried in air at 80ºC. This as-prepared sample was then annealed at 800ºC for 3 hrs. Thus pure hematite nanopowders were obtained. For preparing lanthanum doped hematite nanopowders, 1% of Lanthanum nitrate was dissolved in the mixture of deionized water and ethylene glycol.

2.2. Characterization

X-ray powder diffraction (XRD) patterns of pure and doped α-Fe_2O_3 powder samples were obtained using PANalytical-X'pert Pro X-ray diffractometer with Cu k_α radiation at room temperature (λ=1.5460 Å). Fourier Transform Raman spectra were measured by BRUKER RFS 27 FT-Raman spectrometer with Nd:YAG laser source. Morphological studies of pure sample was carried out using JEOL JSM-6390 SEM operated at an accelerating voltage of 20 kV and that of doped sample was done by using JEOL JSM-7600F FEG-SEM operated at an accelerating voltage of 5 kV. The optical absorption spectra were taken on a Varian Cary 5000 UV–visible spectrometer.

3. Results and Discussion

3.1. X-Ray diffraction Analysis

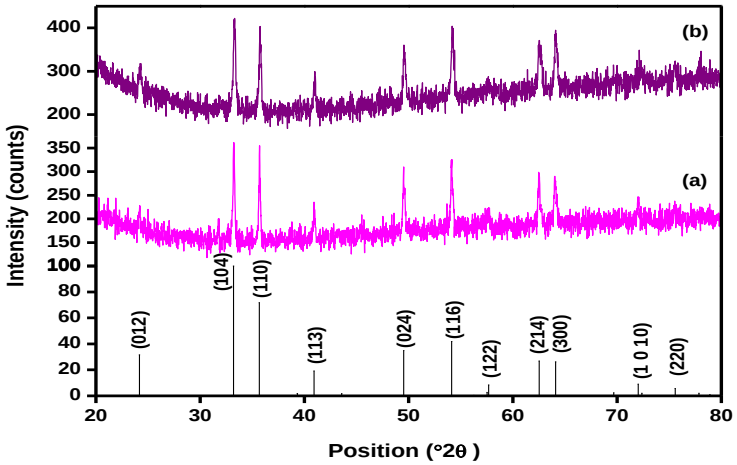

Fig. 1 XRD patterns of the prepared hematite nanopowders: (a) pure (b) La doped

Table 1 Structural parameters of hematite nanopowders

Sample Details	2θ Position	Lattice Parameter	Unit cell volume x10^6 pm^3	Density g/cm^3	Crystallite Size nm	Dislocation density x10^{16} lines/m^2	Micro strain
Standard value	33.198	a = 5.0285 Å c = 13.7360Å	300.79	5.29	-	-	-
Pure	33.2374	a = 5.0345 Å c = 13.7313Å	301.402	5.277	50	0.4072	0.0024
Doped	33.2571	a = 5.0310 Å c = 13.7204Å	300.743	5.2886	36	0.7511	0.0033

The XRD patterns of the pure and La doped α-Fe_2O_3 samples prepared using starting precursors maintained at pH=3 are shown in Fig. 1. All the peaks obtained at the specified locations in the 2θ axis can be indexed as α-Fe_2O_3 based on the JCPDS standards (PDF file no. 01-079-0007) and they are in good agreement with the standard values [14-16]. No peaks of impurities were detected, indicating the purity of the synthesized α-Fe_2O_3. The strong and sharp diffraction peaks of the XRD patterns suggested that the prepared samples are well crystalline and has nano sized grains. The most intense peaks observed at about 2θ=33.2° correspond to the (104) plane. There is a small shift in this peak to the higher angle side in the doped sample and it validates the perfect incorporation of La ions in the α-Fe_2O_3 lattice by replacing Fe ions. Moreover, the present level of doping does not modify the hexagonal unit cell.

The unit cell of α-Fe_2O_3 is hexagonal and contains only octahedrally coordinated Fe^{3+} ions in the pure sample (corundum structure) [17, 18]. Based on the hkl values, the structural parameters were calculated for its hexagonal structure and are listed in Table 1.The lattice parameters of the pure α-Fe_2O_3 sample are very close to the standard values and the incorporated dopant ions modify the cell edge that is compressed along both the a and c axes. Therefore, the unit cell volume is reduced and hence there is an increase in density. Since the dopant cation diameter is not similar to the native cation, the dislocation density and microstrain values increases. The crystallite size also reduces on doping.

3.2. FT-Raman spectroscopy

α-Fe_2O_3 belongs to D^6_{3d} point symmetry group and there exists seven Raman active modes, two vibrations of A_{1g} and five E_g [19]. The mode at 225 cm^{-1} in the bulk material has $A_{1g}(1)$ symmetry, the 245 cm^{-1} is an Eg (2), the 290 cm^{-1} is an E_g (3) + E_g(4), the 409 cm^{-1} mode is E_g(5), the mode at 500 cm^{-1} is A_{1g}(6) and the mode at 612 $cm^{-1}$is E_g (7). The existence of a mode at 1295 cm^{-1} has been assigned to a two magnon mode. Fig. 2 shows the FT-Raman spectra of the pure and lanthanum doped samples.

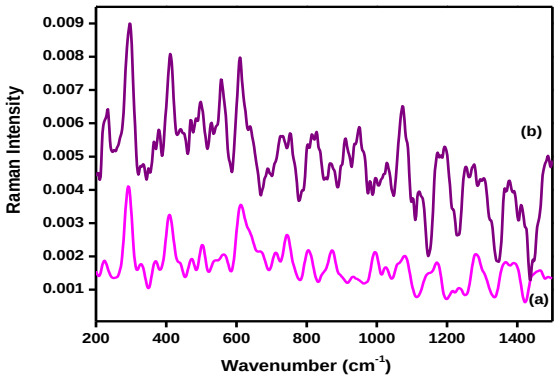

Fig. 2 FT-Raman spectra of the hematite nanopowders (a) pure (b) La doped

The Raman active modes in the pure sample (Fig. 2a) can be assigned as: A_{1g} (223, 501 cm^{-1}), E_g (293, 412, 614 cm^{-1}). For doped sample (Fig. 2b), the modes can be assigned as A_{1g} (229, 499 cm^{-1}), E_g (293, 413, 613 cm^{-1}). The peak at 1280 cm^{-1} is originated from a two-magnon scattering [20]. The observed Raman modes are in good agreement with the reported values [21-23]. The magnon mode is shifted from 1295 cm^{-1} in the bulk material to 1280 cm^{-1} and broadened in the nanomaterial suggesting the effect of phonon confinement on the mode. The resonance in the nanomaterial is more intense. The phonon confinement relaxes the K=0 selection rule in Raman spectroscopy [23]. Raman spectral analysis once again supports the results obtained through XRD that the synthesized product is nanocrystalline Fe_2O_3.

3.3. SEM Analysis

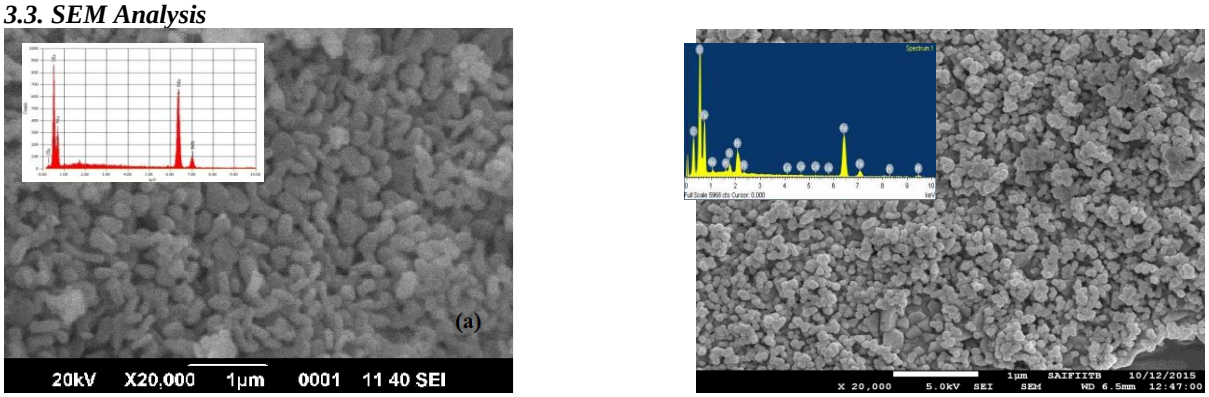

Fig. 3 SEM images of the hematite nanopowders: (a) pure (b) La doped

The morphologies of the prepared samples were studied by SEM and Fig. 3 shows the SEM images of the pure and doped hematite nanopowders. The particles of the pure sample are fine and uniform, forming nearly spherical shape. The size distribution is almost uniform and the calculated average particle size is about 155 nm. In the case of doped sample, the average particle size is 74 nm and the particles are spherical in shape. Obtained particle size values are higher than that obtained through XRD studies, however the size reduction is clearly seen through the SEM images. The composition of the samples was identified from the EDAX spectrum shown as an inset. Pure α-Fe_2O_3 nanoparticle has x-ray absorption peaks corresponding to the elements Fe and O. However in the doped sample, additional peaks corresponding to the element La is visible along with Fe and O. The study further confirms the impregnation of the dopant ion into the Fe_2O_3 lattice.

3.4. UV-Vis spectroscopy

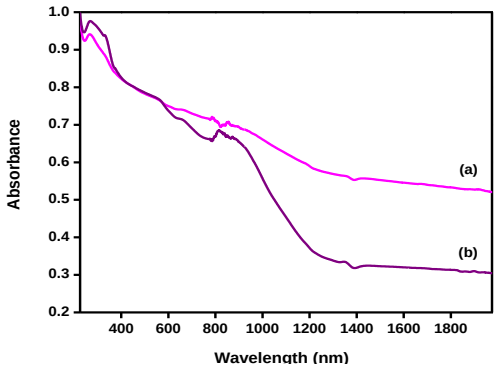

Fig. 4 UV-vis absorption spectra of the hematite nanopowders (a) pure (b) La doped

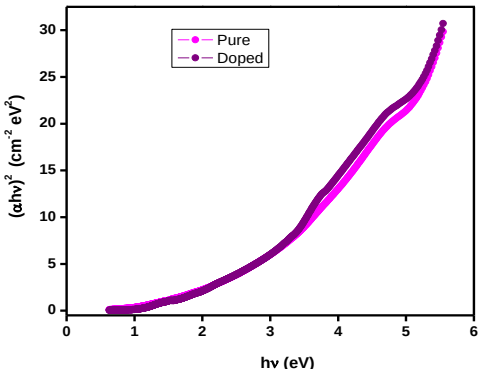

Fig. 5 Variation of $(\alpha h\nu)^2$ vs. photon energy

Fig. 4 shows the optical absorption spectra at room temperature of the pure and lanthanum doped samples. The specific absorption located at 270 nm can be assigned to metal to ligand charge transfer interactions and partly due to the Fe3+ ligand field transitions $^6A_1 \rightarrow {}^4T_1(4P)$. This absorption intensity of the La doped hematite nanoparticles is higher than that of the pure sample. The absorption peak at 540 nm is mainly due to the $^6A_1 + {}^6A_1 \rightarrow {}^4T_1(^4G) + {}^4T_1(^4G)$ excitation of an Fe^{3+}–Fe^{3+} pair, overlapped with the contributions of $^6A_1 \rightarrow {}^4E$, $^4A_1$ (^4G) ligand field transition and the charge-transfer band tail [15]. It has already been reported that α-Fe_2O_3 exhibits both direct and indirect band gaps [24, 25]. The direct and indirect band gap energy (E_g) is estimated using the Tauc equation, $(\alpha h\nu)^{1/n} = B\,(h\nu - E_g)$, where hν is the incident photon energy, α is the absorption coefficient, B is a material-dependent constant and E_g is the optical band gap. The value of n depends on the nature of transition. For direct allowed transition, n=1/2 and for indirect allowed transition n=2. Tauc plots drawn by taking $(\alpha h\nu)^{1/n}$ along the y-axis and hν along the x-axis is shown in Fig. 5 and 6.

Table 2 Band gap values of the hematite nanopowders

Nature of transition	Literature value [26]	Pure	Doped
Direct	2.6 eV	2.47 eV	2.51 eV
Indirect	1.9 eV	1.22 eV	1.18 eV

The average optical band gap is found by extrapolating the linear portion of the curve. The average band gap of the bulk α-Fe_2O_3 is 2.1 eV [15]. The literature values and the calculated values of direct and indirect optical band gap energy of pure and doped hematite nanopowders are listed in Table 2. The calculated values of band gap are found to be in agreement with the literature values. Since the crystallite sizes are different, the band gap values for the pure and doped sample are different.

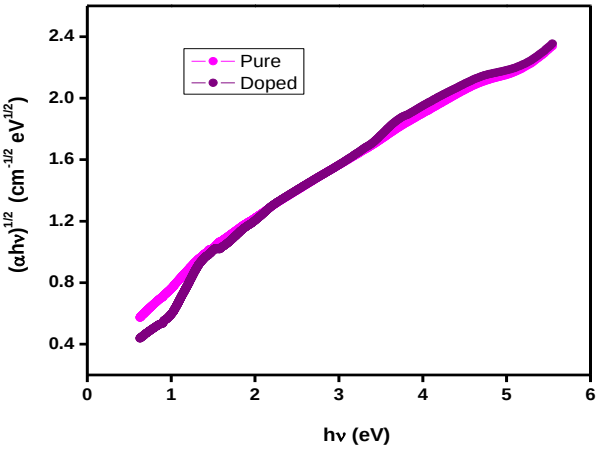

Fig. 6 Variation of $(\alpha h\nu)^{1/2}$ vs. photon energy

4. Conclusion

Pure and lanthanum doped α-Fe_2O_3 nanoparticles were prepared by a facile solution method by simply controlling the pH value of the starting precursor solution. Prepared Fe_2O_3 nanoparticles are phase pure and the present level of La doping has not altered the crystalline structure. Incorporation of the dopant ion into the lattice was identified from the XRD studies and confirmed through FT-Raman and EDAX studies. These results showed the perfect replacement of Fe ions by La ions and the La ions are not seated in the interstitial sites. The phonon confinement of both the samples is evidenced from the FT-Raman studies. Surface morphological studies confirmed the induced alteration in shape, size and distribution of the crystallites due to the dopant ion. Both the direct and indirect band gap changes on replacing the native Fe ions with La ions.

Acknowledgements

We thank Sophisticated Test and Instrumentation Centre, Cochin University, Kerala for their assistance in using SEM and UV-vis facilities. We thank Sophisticated Analytical Instrument Facility, IIT Madras, Chennai for conducting FT-Raman measurements. We are also grateful to Sophisticated Analytical Instrument Facility, IIT Bombay, Mumbai for providing FEG-SEM facility.

References

[1] S. B. Kanungo, S. K. Mishra, Thermal dehydration and decomposition of $FeCl_3.xH_2O$, J. Thermal Analysis 46 (1996) 1487-1500.

[2] Y. P. He, Y. M. Miao, C. R. Li, S. Q. Wang, L. Cao, S. S. Xie, G. Z. Yang, B. S. Zou, Size and structure effect on optical transitions of iron oxide nanocrystals, Physical review B 71 (2005) 125411.

[3] B. K. Pandey, A. K. Shahi, Jyoti Shah, R. K. Kotnala, Ram Gopal, Optical and magnetic properties of Fe_2O_3 nanoparticles synthesized by laser ablation/fragmentation technique in different liquid media, Applied Surface Science 289 (2014) 462-471.

[4] R. D. Zysler, D. Fiorani, A. M. Testa, Investigation of magnetic properties of interacting Fe_2O_3 nanoparticles, Journal of Magnetism and Magnetic Materials 224 (2001) 5-11.

[5] M. Chirita, I. Grozescu, Fe_2O_3 – Nanoparticles, Physical Properties and Their Photochemical And Photoelectrical Applications, Chem. Bull. "POLYTECHNICA" univ. (Timisoara) 54(68) (2009) 1-8.

[6] Norihito Kijima, Masashi Yoshinga, Junji Awaka, Junji Akimoto, Microwave synthesis, characterization and electrochemical properties of α-Fe_2O_3 nanoparticles, Solid State Ionics 192 (2011) 293-297.

[7] F. Vetrone, R. Naccache, V. Mahalingam, C. G. Morgan, J. A. Capobianco, The active-core/active-shell approach: A strategy to enhance the upconversion luminescence in lanthanide-doped nanoparticles, Advanced Functional Materials 19 (2009) 2924–2929.

[8] J. Park, M. Baek, E. Choi, S. Woo, J. Kim, Paramagnetic ultrasmall gadolinium oxide nanoparticles as advanced T1 MRI contrast agent: Account for large longitudinal relaxivity, optimal particle diameter, and *in vivo* T1 MR images, ACS Nano 3 (2009) 3663–3669.

[9] S. Fujihara, G. Murakami, T. Kimura, Oxygen deficiency and electrical conductivity of $Nd_{1-x}A_xNiO_{3-y}$(A = alkaline earth) prepared by the low-temperature process, Journal of Alloys and Compounds 243 (1996) 70.

[10] A. Martinez-Juárez, L. Sánchez, E. Chinarro, P. Recio, C. Pascual, J. R. Jurado, Electrical characterisation of ceramic conductors for fuel cell applications, Solid State Ionics 135 (2000) 525.

[11] D. M. A. Melo, M. A .F. Melo, A. E. Martinelli, Z. R. Silva, J. D. Cunha, A. C. Lima, Synthesis and characterization of lanthanum- and yttrium-doped Fe2O3 pigments, Cerâmica 53 (2007) 79-82.

[12] Francesca Stefania Freyria, Gabriele Barrera, Paola Tiberto, Elena Belluso, Davide Levy, Guido Saracco, Paolo Allia, Edoardo Garrone, Barbara Bonelli, Eu-doped α-Fe_2O_3 nanoparticles with modified magnetic properties, Journal of Solid State Chemistry 201(2013) 302–311.

[13] Gaurav Goyal, Anjana Dogra, S. Rayaprol, S. D. Kaushik, V. Siruguri, H. Kishan, Structural and magnetization studies on nanoparticles of Nd doped α -Fe_2O_3, Materials Chemistry and Physics 134 (2012) 133– 138.

[14] Chun-Yang Yin, Manickam Minakshi, David E.Ralph, Zhong-Tao Jiang, Zonghan Xie, Hua Guo, Hydrothermal synthesis of cubic α-Fe_2O_3 nanoparticles using glycine: Surface characterization, reaction mechanism and electrochemical activity, Journal of Alloys and Compounds 509 (2011) 9821-9825.

[15] Maryam Mohammadikish, Hydrothermal synthesis, characterization and optical properties of ellipsoid shape α-Fe_2O_3 nanocrystals, Ceramics International 40 (2014) 1351–1358.

[16] Xun-Liang Cheng, Ji-Sen Jiang, Chuan-Yin Jin, Chu-Chen Lin, Yi Zen, Qin-Lang Zhang, Cauliflower- like α-Fe_2O_3 microstructures: Toluene-water interface-assisted synthesis, characterization and applications in wastewater treatment and visible-light photocatalysis, Chemical Engineering Journal 216 (2014) 139-148.

[17] F. Wang, X.F. Qin, Y.F. Meng, Z.L. Guo, L.X. Yang, Y.F. Ming, Hydrothermal synthesis and characterization of α-Fe_2O_3 nanoparticles, Materials Science in Semiconductor Processing 16 (2013) 802–806.

[18] S.K. Sahoo, K. Agarwal, A.K. Singh, B.G. Polke, K.C. Raha, Characterization of γ- and α-Fe_2O_3 nano powders synthesized by emulsion precipitation-calcination route and rheological behavior of α-Fe_2O_3, International Journal of Engineering, Science and Technology 2 (2010) 118-126.

[19] N.D. Phu, D.T. Ngo, L.H. Laang, N.H. Luong, N.H. Hai, Crystallization process and magnetic properties of amorphous iron oxide nanoparticles, Journal of Physics D: Applied Physics 44 (2011) 345002.

[20] K.F. McCarty, Inelastic light scattering in α-Fe_2O_3: Phonon vs magnon scattering, Solid State Communications 68 (1988) 799-802.

[21] Sang-Heon Shim, Thomas S. Duffy, Raman spectroscopy of Fe_2O_3 to 62 GPa, American Mineralogist, 87 (2001) 318-326.

[22] I.R. Beatie, T.R. Gilson, The single-crystal Raman spectra of nearly opaque materials. Iron (III) oxide and chromium (III) oxide, Journal of Chemical Society A5 (1970) 980-986.

[23] M.J. Massey, U. Baeir, R. Merlin, W.H. Weber, Effects of pressure and isotopic substitution on the Raman spectrum of α-Fe_2O_3: Identification of two-magnon scattering, Physical Review B 41 (1990) 7822-7827.

[24] M.F. Al-Kuhaili, M. Saleem, S.M.A. Durrani, Optical properties of iron oxide (α-Fe_2O_3) thin films deposited by the reactive evaporation of iron, Journal of Alloys and Compounds 521 (2012) 178-182.

[25] A.A. Akl, Optical properties of crystalline and non-crystalline iron oxide thin films deposited by spray pyrolysis, Applied Surface Science 233 (2004) 307-319.